Proof of quark confinement and baryon-antibaryon duality: I: Gauge symmetry breaking in dual 4D fractional quantum Hall superfluidic space-time

A. E. Inopin[1] and N. O. Schmidt[2]

[1] *Department of Experimental Nuclear Physics, Karazin National University, Svobody Sq. 4, Kharkiv, 61077, Ukraine (E-mail: inopinandrej@yahoo.com)*
[2] *Department of Mathematics, Boise State University, 1910 University Drive, Boise, Idaho, 83725, USA (E-mail: nathanschmidt@u.boisestate.edu)*

(Dated: October 2012)

We prove quark (and antiquark) confinement for a baryon-antibaryon pair and design a well-defined, easy-to-visualize, and simplified mathematical framework for particle and astro physics based on experimental data. From scratch, we assemble a dual 4D space-time topology and generalized coordinate system for the Schwarzschild metric. Space-time is equipped with "fractional quantum number order parameter fields" and topological defects for the simultaneous and spontaneous breaking of several symmetries, which are used to construct the baryon wavefunction and its corresponding antisymmetric tensor. The confined baryon-antibaryon pair is directly connected to skyrmions with "massive 'Higgs-like' scalar amplitude-excitations" and "massless Nambu-Goldstone pseudo-scalar phase-excitations". Newton's second law and Einstein's relativity are combined to define a Lagrangian with effective potential and effective kinetic. We prove that our theory upgrades the prediction precision and accuracy of QCD/QED and general relativity, implements 4D versions of string theory and Witten's M-theory, and exemplifies M.C. Escher's duality.

I. INTRODUCTION

Quarks and antiquarks are the fundamental building blocks of baryons and antibaryons, respectively. To date, nature presents an impressive display of mass-energy puzzles in physics, including the creation, annihilation, and confinement of baryons and antibaryons. The mystery of quark confinement is a *colossal* problem in physics; it is the phenomenon that color charged particles (such as quarks) cannot be isolated singularly, and therefore cannot be directly observed [1]. In this first paper of the series, we hunt down this "Great Beast" and prove quark-antiquark confinement for a baryon-antibaryon pair in a 4D space-time, where the dimension of time is circular rather than linear. We attack the problem from multiple perspectives simultaneously to establish a well-defined gauge theory equipped with Legget's superfluid configuration of Landau's order parameter fields [2], Laughlin's quasiparticles [3], a baryon wavefunction, antisymmetric tensors, and more. From scratch, we construct a topological solution and Lagrangian that intertwines Newtonian [4] and Einsteinian concepts [5], improves the predictive capability of quantum chromo-dynamics (QCD) and quantum electro-dynamics (QED) [6], reduces dimensional complexity of string theory and M-theory [7], exhibits M.C. Escher's duality [8], and is directly supported by a diverse experimental array. In short, the *dual* baryon and antibaryon quantum states are encoded with quantum number order parameters of fractional statistics for quasiparticles with baryon wavefunction antisymmetry. We prove quark-antiquark confinement in terms of Laughlin excitations [3] that dynamically arise due to our *fractional quantum Hall superfluidic* (FQHS) space-time and topology inspired by the quasiparticle interferometer experiments of Goldman [9]. We prove that the quarks and antiquarks confined to the holographic ring "cancel out" due to the CPT-Theorem. Spontaneous symmetry breaking (SSB) generates massless "Nambu-Goldstone pseudo-scalar *phase-excitations*" [10–13] and massive "Higgs-like scalar *amplitude-excitations*" [14] of Laughlin statistics [3]. First, we provide *conceptual* quark confinement proof in Section II. Second, we provide *mathematical* quark confinement proof in Sections III, IV, V, and VI.

In Section II, we prepare for our quark confinement proof by conceptually aligning the reader to our 4D FQHS space-time scenario. We investigate the two dynamical scales that arise in the double-confinement, double-stereographic gravitational superlensing, and double-horizons inherent to baryons and antibaryons. We prove that a baryon-antibaryon pair is composed of three distinct quark-antiquark pairs, which form three corresponding "thin color-electric flux tubes" [15] of Laughlin excitations [3] and fractional statistics [16]. We discuss the hadronization process and the modified Gribov QED/QCD vacuum, where all properties in 3D Schwarzschild space can be inferred from the analogue of the 2D gauge field on the six-coloring kagome lattice manifold. Additionally, we venture to the interaction between the boson propagators and gravity by introducing *"gravitational birefringence"*.

In Section III, we begin mathematically constructing the topology and framework for our quark confinement proof in FQHS. We discuss the surface and generalized Riemann coordinates used to encode our FQHS space-time. We extend the definition of complex numbers and use them to represent locations on the 1D Riemann surface; we prove that the complex numbers are both scalars and Euclidean vectors. We define axis constraints for the vectors, which let us construct a powerful 2D generalized coordinate system on the surface equipped with the Pythagorean identity; the locations may always be

expressed in terms of right triangles with real and imaginary components.

In Section IV, we explore the three distinct topological sub-surface zones for a baryon and antibaryon using set and group theory. We formally define the zones using trichotomy and our generalized coordinates for 2D and 3D space. We prove that the time-like region is a holographic ring—a closed curve and simple contour of points, which can be scaled to, for example, the Fermi radius. We formally define space and time as being dual. Additionally, we demonstrate that the time-like region represents the $U(1)$ and $SU(2)$ symmetry groups, which is isomorphic to the $SO(3)$ orthogonal group; all 3D properties are inferred directly from the 2D holographic ring for the $SU(2)$ gauged Bose-Einstein condensate.

In Section V, we define the *Baryon Wavefunction* (BWF) of fractional quantum number order parameters (OP) for our quark (q) and antiquark ($\bar{q}$) confinement proof. Additionally, we discuss the amplitude-excitations [14] and phase-excitations [10–13] for Laughlin quasiparticles [3] experienced by the BWF OPs in our FQHS space-time scenario. For this, we express the full BWF antisymmetries and CPT-transformations.

In Section VI, we express the Lagrangian in terms of *effective potential* and *effective kinetic* for our FQHS space-time scenario. For this, we apply both Newtonian and Einsteinian concepts to the q and $\bar{q}$ confinement proof and thereby incorporate *effective force*, *effective mass*, and *effective acceleration*.

In Section VII, we prepare a concise correspondence to the authors of the Yuan-Mo-Wang (YMW) baryon-antibaryon $SU(3)$ model [17]. In doing so, we relay the importance of the YMW model and report on a number of similarities between it and our confinement scenario. Additionally, we contrast the models by identifying key distinctions and suggest that our model may upgrade the YMW model's state space and accuracy, and thereby extend its prediction horizon. Ultimately, we realize that both constructions exhibit remarkable similarities, and that it may be possible in the near future to consolidate these ideas into a single framework.

In Section VIII, we conclude our paper with a brief recapitulation and outlook where we suggest future research trajectories.

To summarize, in this first paper of the series we introduce the topologies, vacuum, generalized coordinates, fractional statistics, quantum number OPs, BWF, gauge symmetry breaking, and Lagrangian for the q and $\bar{q}$ confinement proof in 4D FQHS space-time; for the scenario, we provide a series of colorful depictions and an array of experiments supporting this construction. In the next paper(s) of this series, we will extend our confinement scenario by discussing the anyons, phase locking [18], Hubius helix (HH) [19], attractive and repulsive gravitational effects of quasiparticle signals on the Lagrangian, modified Gullstrand–Painlevé reference frames, and Magnification Effect.

II. ALIGNMENT TO CONFINEMENT: CONCEPTUAL PROOF

At the Fermi scale, a baryon's event horizon confinement radius $\epsilon_{baryon} = 2M_{baryon}$ strongly depends on it's mass M_{baryon}, which can vary in size in accordance to its quark composition identified by the Standard Model. This is known as *baryon confinement* (for three-quark confinement) and is modeled as a *baryon bag*. Similarly, an antibaryon's event horizon confinement radius $\epsilon_{antibaryon} = 2M_{antibaryon}$ strongly depends on it's mass $M_{antibaryon}$. This is known as *antibaryon confinement* (for three-antiquark confinement) and is modeled as an *antibaryon bag*. A baryon and its antibaryon merge to reflect three-pair quark-antiquark confinement. For example in a proton-antiproton pair, an antiproton of antimass $M_{antibaryon} = M_{antiproton} = 1$ GeV precisely counterbalances a proton of mass $M_{baryon} = M_{proton} = 1$ GeV due to antiferromagnetic ordering and the CPT-Theorem. On this scale we identify the general mechanism, namely *Baryon-Antibaryon Confinement* (BAC), which is responsible for the dynamics. It is based on the appearance of a critical radius $\epsilon_{2M} = \epsilon_{baryon} = \epsilon_{antibaryon}$ for quark-antiquark confinement at the 1 Fermi scale and the appropriate generalized dynamics—effective gravitostrong interaction. So in gravity plus electromagnetism, there is one interesting mechanism—radiation trapping just on the horizon's surface, that is a coherent particle accumulation structure [18] of fractional statistics and *toroidal vortex* [20]. The toroidal vortex, that stores information as in the holographic hypothesis [15], intertwines the baryon and antibaryon confinement mechanisms, creating BAC. The toroidal vortex forms between the spherical shells defined at the *inner confinement radius* ϵ_{2M} and the *outer confinement radius* $\epsilon_{3M} = 3M$ (based on the effective potential); ϵ_{2M} and ϵ_{3M} correspond to the "horizon" and "imaginary surface", respectively, in Figure 6 of Witten [15]; there are two distinct quantum critical points imposed by an antibaryon or baryon for the *double-stereographic gravitational superlense* with the meta-material, acoustic, double-negative refractive index, and sub-wavelength features of [21–24]—see Figure 1. These facts are evident from the DIS modeling results of the hadronization process [25]. Quark-hadron duality in jet formation in DIS leads to a two-step process of hadronization, with *two scales* appearing: large $Q_0^2 \gg \Lambda_{QCD}^2$ and small $Q_0^2 \sim 1GeV^2$. An alternative approach in DIS, namely "Local Parton Hadron Duality", also leads to the *two dynamical scales*: $k_\perp = Q_0 \sim \Lambda_{QCD}$ and $k_\perp = Q_0 \sim 1$ GeV [25]. Both models of the hadronization process give us the numbers in accord with our model $\epsilon_{2M} \sim 0.2-0.3$ fm and $\epsilon_{3M} \sim 1$ fm. Another fresh perspective can be taken from the "Glue drops" model [26], where the authors gave firm evidence of the existence of a non-perturbative scale, smaller than the usual $\frac{1}{\Lambda_{QCD}} \sim 1$ fm, which is related to gluonic degrees of freedom. The evidence for the presence of a *semi-hard* scale in hadronic structure is reviewed from

many venues. The most notable effects are: QCD sum rules gives 0.3 fm radius of the corresponding form factor, lattice gives 0.2-0.3 fm for the correlation length, instanton radius peaks approximately at 0.3 fm, diffractive gluon bremsstrahlung in hadronic collisions leads to $k_\perp$ for the gluons in a proton of about 0.7 GeV [27]. At higher scales, chiral symmetry breaking is restored and the vacuum does not feel apparent existence of quark and gluon condensates, which spoil the chiral symmetry from the start—the mechanism for the *spontaneous breaking of chiral symmetry* and *spontaneously emergent behavior* of chaos theory on the Lagrangian.

All together, this brings us to the concept of *Baryon-Antibaryon Duality* (BAD), which is responsible for the stereographic superlensing [23] dynamics. At rest, the massless red, green, and blue quarks are confined to a baryon and circulate *counter-clockwise* along it's event horizon as a *left-handed* HH [19] at the speed of light to generate *effective mass*, such that all observable baryons are *white*; the *visible* colored quarks are *non-Abelian color-electric-magnetic monopoles* [28] which emit red, green, and blue light-rays to render a baryon. Similarly, the resting antired, antigreen, and antiblue antiquarks are confined to a antibaryon and circulate *clockwise* along it's event horizon as a *right-handed* HH [19] to generate *effective antimass*, such that all "observable" antibaryons are *black* (antiwhite); the "visible" anticolored antiquarks are *non-Abelian anticolor-electric-magnetic antimonopoles* [28] which emit antired, antigreen, and antiblue light-rays to render an antibaryon; the relative direction of circulation (with corresponding winding number) distinguishes between mass (i.e. M_{proton}) and antimass (i.e. $M_{antiproton}$). For BAD, the baryon and antibaryon bags are dual, opposite, reverse, and inverse, and are therefore modeled as a *Baryon-Antibaryon Bag* (BAB). The quark and antiquark trajectories follow Wilson loops and form a self-consistent [10] $SU(2)$ gauged Bose-Einstein condensate [29]. The electro-strong duality of the potentials continuously transform in FQHS space-time in accordance with 1D, 2D, and 3D skyrmions [29].

This rich concept of duality enables us to compute observables in time-like regions, given the physics in space-like regions, and vice-versa. Upon considering these dual fields, the idea of *two distance scales* comes up naturally. Our 1D Riemmann surface (2D holographic information structure) is divided into three distinct topological subsurfaces for quasiparticles:

1. *Non-Relativistic Space Zone* (NSZ) or "Micro" distance scale of *superluminal* signals,
2. *Time Zone* (TZ), and
3. *Relativistic Space Zone* (RSZ) or "Macro" distance scale of *luminal* signals.

The Riemannian holographic ring unit circle represents the TZ and is isometrically embedded on the surface; it bifurcates 3D space to establish the NSZ, such that $0 < x < \epsilon_{2M}$, and the RSZ, where $\epsilon_{2M} < x < \infty$—recall Figure 1. The gauge field is a 3D analogue of the TZ's Rashba spin-orbit coupling [29]—see Figure 4. The quarks (and leptons) are "split" into three distinct excitation degrees of freedom, namely spinon, holon, and orbitons [3, 30]; the Laughlin excitations of the FQHS 3-branes obey fractional statistics; luminal quasiparticle signals of the RSZ "sea" execute a closed path around the NSZ "island" of superluminal quasiparticle signals and thus acquire statistical phase [9]—see Figure 5.

In QCD, BAC is a difficult strong coupling problem, but a somewhat similar phenomenon in nature is much better understood in QED. The Meissner effect is the fundamental observation that a superconductor expels magnetic flux. Suppose that magnetic monopoles become available for study and that we insert a monopole-antimonopole pair into a superconductor, where the two poles are separated by a large distance x. What will happen? A monopole is inescapably a source of the magnetic flux, but magnetic flux is expelled from a superconductor. So the optimal solution to this problem, energetically, is that a thin, *non-superconducting* tube forms between the monopole and the antimonopole. The magnetic flux is confined to this region, which is known as an *Abrikosov-Gorkov* flux tube (or a *Nielsen-Olesen* flux tube in the context of relativistic field theory). The flux tube has a certain nonzero energy per unit length, so the energy required to separate the monopole and antimonopole by a distance x grows linearly in x, for large x.

As a non-Abelian gauge theory, QCD has fields rather similar to ordinary electric and magnetic fields but obey a *nonlinear* version of Maxwell's equations. Quarks and antiquarks are particles that carry the QCD analog of electric charge and are confined in our QCD vacuum just as ordinary magnetic charges would be in a superconductor. The color-electric-magnetic quark monopoles and anticolor-electric-magnetic antiquark antimonopoles may be separated by a large distance x to form non-Abelian dipoles: red-antired, green-antigreen, and blue-antiblue "thin color-electric flux tubes" [15]. Now from the Aharonov–Casher (AC) effect and Aharonov–Bohm (AB) effect duality [31–33], it is evident that this analogy immediately leads to the idea that *the QCD vacuum is to a superconductor, just as electricity is to magnetism, and just as the AC effect is to the AB effect*—see Figure 3.

In [34], the author considered a relativistic string model, where a massless quark moves at the speed-of-light in a circular orbit. One can see clearly the $x = x_0 = \epsilon_{2M}$ coordinate represents an event horizon or "impenetrable barrier" and the quark moves in the "half harmonic oscillator" potential. When combined with the phenomenological aspects of [35, 36], a strong QCD/QED string model for the $q\bar{q}$ pairs with the associated quasiparticles [3] emerges in our scenario. So for the $q\bar{q}$ pairs we identify both open-ended ("linear") fermionic strings *and* the closed ("non-linear"/circular) bosonic strings vibrating in our conjugate and dual space-time. All of this

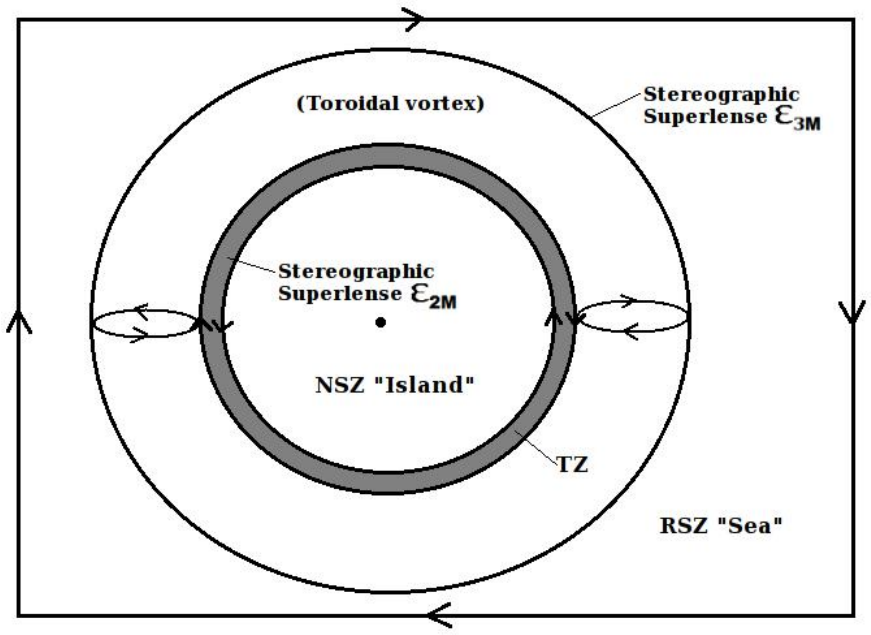

FIG. 1. The Riemannian holographic ring unit circle of two counter-propagating edge channels defines the TZ for quark-antiquark confinement and is isometrically embedded on the 1D Riemann surface. The toroidal vortex between two dynamical scales for a double-stereographic gravitational superlense: the spherical shells located at critical radius $\epsilon_{2M} = 2M$ and $\epsilon_{3M} = 3M$.

is supported by Glue drops [26], where the energy of a QCD string is concentrated in a thin color-electric flux tube [15] of radius $\epsilon_{2M} = 0.3$ fm. All such particles and quasiparticles on the Riemann surface which generate effective mass (and antimass) are projected along the "z-axis" to effective 3D space (recall Figure 4). Here, events are represented on the Lagrangian using generalized coordinates in Schwarzschild space-time on the Riemann surface.

Viewed in certain classes of inertial frames, a superluminal signal travels *backwards* in time. In QED, Feynman diagrams involve a virtual e+e- pair that influences the photon propagator. Here, positrons are replaced with electron-holes. This gives a photon an effective mass (or antimass) on the order of the Compton wavelength for the electron (or electron-hole); leptons are split into quasiparticles [3, 30]. All of this is generalized to QCD, where a virtual $q\bar{q}$ pair influences the gauge boson propagator in FQHS space-time; the propagator is a function which returns a probability amplitude of 1 for the quarks and baryon confined to the TZ. In both QED and QCD, if the space-time curvature has a comparable scale, then an effective boson-gravity interaction is induced; the Higgs-like amplitude excitations [14] for the baryon-antibaryon pair impose effective mass for baryons and quarks, and effective antimass for antibaryons and antiquarks. This depends explicitly on the curvature, in violation of the Strong Equivalence Principle. The boson velocity is changed and light-ray no longer follows the shortest possible path—it bifurcates to both the NSZ and RSZ distance scales. Moreover, if the space-time is anisotropic, this change can depend on the boson's polarization as well as direction. This is the quantum phenomena of "gravitational birefringence". The effective light-cones for boson propagation in gravitational fields *no longer coincide* with the geometrical light-cones fixed by the local Lorentz invariance of space-time, but depend *explicitly* on the local curvature. This formulation agrees with the von Karman flow and symmetry breaking of [37], the kaleidoscope of exotic quantum phases in the 2D frustrated model of [38], and the deviant Fermi liquid of [39], where the TZ serves a Bose metal as in [40]. All this works in 4D space-time.

The $q\bar{q}$ pairs for a baryon-antibaryon pair are "superbound" to the vacuum [41] as coupled oscillators [42] (see Figure 2) and form red-antired, green-antigreen, and blue-antiblue *Nambu-Goldstone pions*, which are Nambu-Goldstone bosons; the SSB of the three distinct pions generates colored amplitude-excitations [14] and phase-excitations [10–13]. The $q\bar{q}$ pairs of the three distinct thin color-electric flux tubes are confined to the TZ, which is a *Riemannian holographic ring unit circle* on a 1D Riemann surface equipped with a six-coloring (three coloring plus three anticoloring) kagome lattice manifold generalization of [43] with antiferromagnetic ordering [3]. The ring exhibits the Rashba and fractional quantum Hall effects [44], along with spin-Hall current [45] and chiral magnetic moments [46]. The $q\bar{q}$ pairs are uniformly arranged along the kagome lattice with the triangular chirality of [47] and the self-assembling observables of [18, 48] (recall Figure 3). The quasiparticles of the $SU(2)$ gauged Bose-Einstein condensate are direct 3D analogs of

the spontaneously emerging QED and QCD. The kagome lattice hexagonal structure is self-similar to, for example, graphene, which explains the "plasmaron" observations in quasi-freestanding doped graphene [49] and the "soundaron" observations of [50]. The quarks can also be thought as moving along the "caustics" inside the toroidal vortex, where the quark's trajectories are trapped between the dual scale dynamics—they are "gliding" along the surface and are reflected back to the center. The dual confinement boundaries located at ϵ_{2M} and ϵ_{3M} act as reflecting and focusing stereographic superlenses. So baryons and antibaryons become *seashells* closed on ϵ_{3M} [51].

When we come to the vacuum estate, the richness of BAD is shining brightly: Gribov's QED/QCD vacuum [41] resembles a complicated structure of *Unruh-Boulware-Hartle-Hawking*'s black hole vacuum and is fed with solid-state physics along with notions of forbidden zones, Fermi surfaces, particles and holes to encode the BAB on the Riemann surface. But there are some new diagrams that arise with the new zones, and novel types of excitations—enabling us to upgrade Gribov's model. This new vacuum differs drastically from Dirac's vacuum and contains a total of 18 zones for the six-coloring (kagome lattice) manifold on the Riemann surface—Figure 4; these zones are populated with quasiparticles [3, 30] spontaneously generated by the $q\bar{q}$ pairs confined to the TZ with the spin-orbit coupling of [45, 53–55]. The TZ acquires a geometric phase [31, 32, 56], so the quasiparticles confined to the TZ are dual to those signals propagated across the NSZ and RSZ zones. Laughlin's fractional quantization [16] is axiomatic in this scenario. At proper temperature and pressure, the vacuum is consistent with Chernodub [57]. Clearly, in treating the BAD and superlensing dynamics, it is very convenient to separate the RSZ and NSZ degrees of freedom (Born–Oppenheimer approximation).

The NSZ and RSZ both represent *superconductive, FQHS* 3-*branes* interconnected by the TZ, which serves as a common (2D) surface boundary at ϵ_{2M}. The baryon and antibaryon are spinning objects confined to the TZ so they generate whirlpools on both 3-brane distance scales in accordance with seashells closed on ϵ_{3M} [51], thereby exhibiting the Magnus effect [58] and generating a vortex-antivortex dance [52]; these whirlpools are described on the Riemann surface using spirals (i.e. weighted Fibonacci sequence and/or golden spiral). The TZ is a topological Mott insulator for [30, 53, 59, 60], a Fermi surface as in [61], a Goldman-Laughlin quasiparticle interferometer of two counter-propagating edge channels as in [9], a Gedanken interferometer as in [62], a quantum critical point as in [3, 63], and a non-perturbative, self-consistent, $SU(2)$ gauged Bose-Einstein condensate as in [10] that satisfies Novikov's self-consistency principle as in [64]; a picture emerges of the vacuum as a conductor instead of "Dirac's insulator", with a new mass scale that reflects the position of the "Fermi surface" [41]. The six-coloring antiferromagnetic alignment of the $q\bar{q}$ pairs spontaneously generate the physical behavior of the strong interaction as in [3] and thereby triggers parity doubling, CPT violations, and different polarization rotation velocities on *both* the NSZ and RSZ distance scales simultaneously. Here, we identify the Dirac quantization and spin-charge magnetic monopole relations of [65], Fermi liquid deviations of [63], non-linear optics, analogue gravity, and photon emissions analogous to the Hawking radiation as in [66], and Andreev reflections of [67, 68]; the TZ's current continuously undergoes charge-transformation between the NSZ's and RSZ's supercurrent. The $q\bar{q}$ resonances form the exotic meson and broad locking states as in [69]. The $q\bar{q}$ pairs and their waves are phase locked, spontaneously aligning to form dynamical 1D coherent accumulation structures with time-periodic flows [18] and a von Kármán vortex street [20] with impact parameters.

III. THE SPACE-TIME SURFACE AND GENERALIZED RIEMANN COORDINATES

Let X be the 1D Riemann surface. We define the complex number $x = x_{\mathbb{R}} + x_{\mathbb{I}}$ as a *position-point and position-vector* on X; $x \in X$ is both a complex scalar *and* Euclidean vector with *amplitude* $|x|$ and *phase* $\langle x \rangle$, which are analogous to *magnitude* and *direction* in conventional notation. The orthogonal components of x, namely $x_{\mathbb{R}} \in \mathbb{R}^1$ and $x_{\mathbb{I}} \in \mathbb{I}^1$ as *axis-constrained* real and imaginary Euclidean vectors, respectively (where in this case $\mathbb{I}$ denotes imaginary rather than irrational); the simple trichotomy axis-constraints for the $\mathbb{R}$-axis are

$$x_{\mathbb{R}} > 0 \Leftrightarrow \langle x_{\mathbb{R}} \rangle = 2\pi = 0, \tag{1}$$
$$x_{\mathbb{R}} = 0 \Leftrightarrow \langle x_{\mathbb{R}} \rangle = \nexists, \tag{2}$$
$$x_{\mathbb{R}} < 0 \Leftrightarrow \langle x_{\mathbb{R}} \rangle = \pi, \tag{3}$$

and for the $\mathbb{I}$-axis are

$$x_{\mathbb{I}} > 0 \Leftrightarrow \langle x_{\mathbb{I}} \rangle = \frac{\pi}{2}, \tag{4}$$
$$x_{\mathbb{I}} = 0 \Leftrightarrow \langle x_{\mathbb{I}} \rangle = \nexists, \tag{5}$$
$$x_{\mathbb{I}} < 0 \Leftrightarrow \langle x_{\mathbb{I}} \rangle = \frac{3\pi}{2}, \tag{6}$$

such that

$$|x_{\mathbb{R}}| = |x| \cos(\langle x \rangle), \tag{7}$$
$$|x_{\mathbb{I}}| = |x| \sin(\langle x \rangle), \tag{8}$$

with Pythagorean form

$$|x|^2 = x_{\mathbb{R}}^2 + x_{\mathbb{I}}^2, \quad \forall x \in X. \tag{9}$$

Thus, we've defined the 2D generalized (Riemann) coordinate system of X as

$${}^{2D}X : (x) = (x_{\mathbb{R}} + x_{\mathbb{I}}) = (x_{\mathbb{R}}, x_{\mathbb{I}}) = (|x|, \langle x \rangle), \quad \forall x \in X, \tag{10}$$

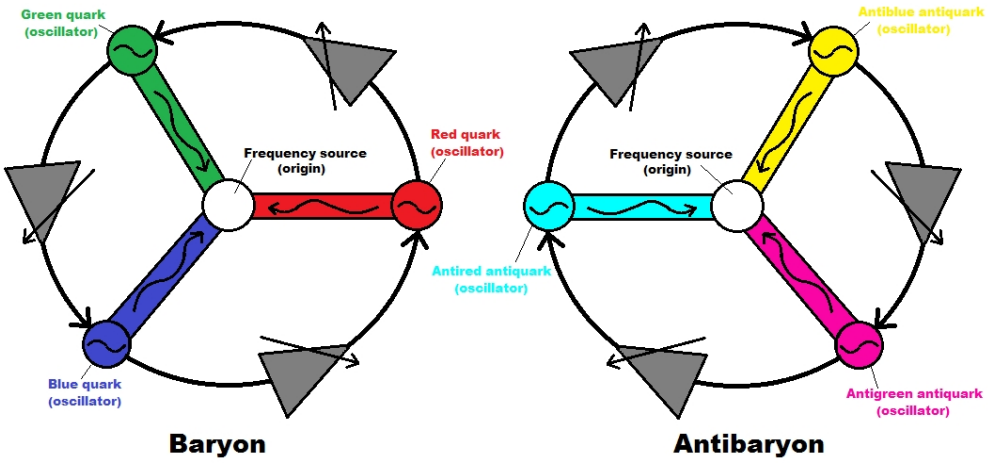

FIG. 2. Schematic of the multiple synchronized quark and antiquark solid-state oscillators (colored and anticolored circles) coupled to generate frequencies for the $SU(2)$ gauged Bose-Einstein condensate with skyrmions [29] in the loop configuration based on the work of Afshari [42]; the coupling circuits (gray triangles) shift the phase of the oscillators.

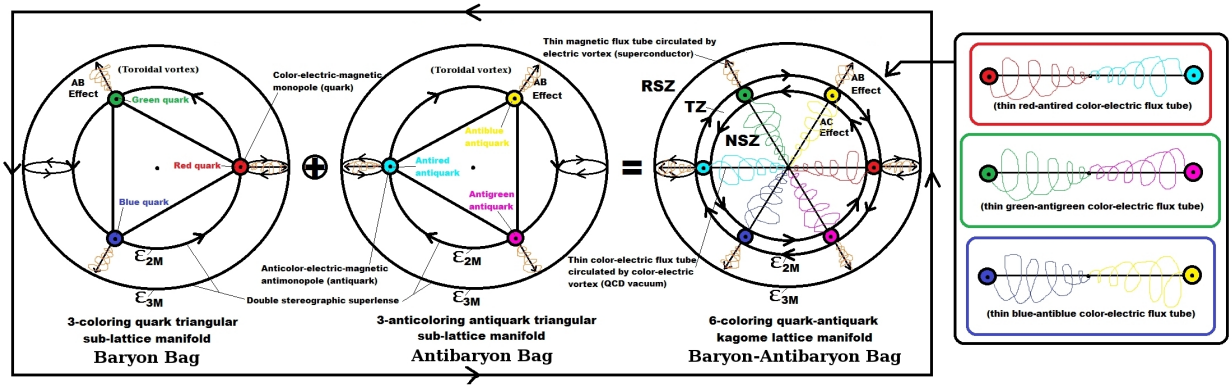

FIG. 3. The loop-induced zero-energy dynamics are described as "gluon dynamics". The 3 distinct $q\bar{q}$ pairs for the baryon-antibaryon pair are "superbound" as coupled oscillators [42] to the Fermi surface in the upgraded Gribov vacuum generalized from [41] and are confined to the kagome lattice antiferromagnet on the six-coloring manifold. The $q\bar{q}$ pairs spontaneously generate *phase-excitations* (massless and pseudo-scalar) [10–13] and "Higgs-like" *amplitude-excitations* (massive and scalar) [14] Laughlin excitations [3]. The toroidal vortex along the Riemannian holographic ring unit circle for a baryon and/or antibaryon is defined as a toroidal vortex between the spherical shells located at critical radius $\epsilon_{2M} = 2M$ and $\epsilon_{3M} = 3M$; double stereographic superlenses [23] for two dynamical scales [27]. An affinity exists between BAD and M.C. Escher's duality, where the combined baryon event horizon and antibaryon event horizon at ϵ_{2M} exhibit the double horizon phenomena [8]. The $q\bar{q}$ pairs confined to the TZ form thin color-electric flux tubes [15] in the QCD vacuum of the NSZ and exhibit the AC effect, while thin magnetic flux tubes in the RSZ superconductive region exhibit antiferromagnetic ordering and the AB effect; the QCD vacuum is to a superconductor, just as electricity is to magnetism, and just as the AC effect is to the AB effect. This model exhibits vortex-antivortex dancing [52] and confirms the spontaneous appearance of a stable 3D skyrmion in the $SU(2)$ gauged Bose-Einstein condensate of [29] confined to the Riemannian holographic ring unit circle on our 1D Riemann surface.

with respect to the unique reference origin-point $O \in X$, such that $(O) = (0 + 0i) = (0, 0i) = (0, 0\pi)$; $(x) = (x_{\mathbb{R}} + x_{\mathbb{I}})$ are 1D Riemann coordinates, $(x_{\mathbb{R}}, x_{\mathbb{I}})$ are 2D Cartesian coordinates, and $(|x|, \langle x\rangle)$ are Polar coordinates; a Complex-Cartesian-Polar synchronized and generalized coordinate system. The real and imaginary axis-constraints ensure that the generalized coordinates may always be expressed as a right-triangle with Pythagorean properties.

So how to we extend our 2D generalized coordinates of Definition (10) to 3D Schwarzschild space? Well, for a baryon or antibaryon of scale M (located precisely at the origin position-point $O \in X$) we define the 3D generalized (Schwarzschild) coordinate system of X as

$$^{3D}X : (u_x, |x|, \langle x\rangle) = (\frac{M}{|x|}, |x|, \langle x\rangle), \quad \forall x \in X. \qquad (11)$$

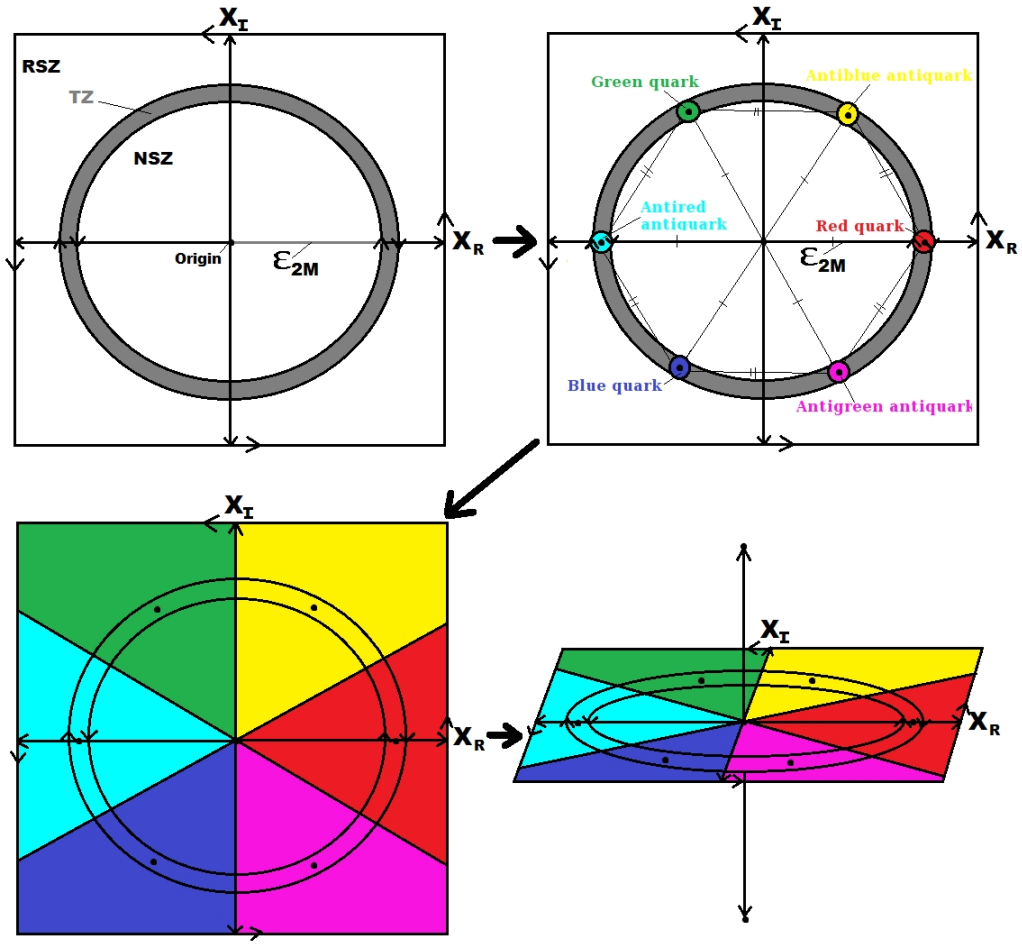

FIG. 4. The gauge-invariant TZ delineates the NSZ and RSZ: a 2-sphere which is dual to *both* 3-branes, where the $SU(2)$ Bose–Einstein condensate and gauge field is a 3D analogue of the Rashba spin-orbit coupling of the TZ, supporting the 1D, 2D, and 3D Skyrmion structures [29] (all). The baryon-antibaryon pair comprises the three distinct $q\bar{q}$ pairs and is modeled as a BAB in the new Gribov vacuum with 18 quasiparticle signal zones (bottom).

IV. ZONES

We define T as the TZ of X. So T is a topological representation of a Riemannian unit circle, where the critical radius of T is scaled and normalized to precisely $\epsilon_{2M} = 2M = \frac{\pi}{2}\epsilon_{scalar}$. We prove BAC on T. ϵ_{scalar} is the *time unit scale-normalizing constant* and ϵ_{2M} is the inner confinement radius of T. Next, we define the circumference and wavelength of T, namely $T_\lambda = T_{circumference} = T_{wavelength} = 2\pi\epsilon_{scalar}$, as being equivalent to the (normalized) *Mikhail Grimov's area filling conjecture* [70]: $T_{area} = T_\lambda$; $T \subset X$ is a closed curve and simple contour of surface position-points.

We use zone trichotomy to simultaneously define the TZ and SZ regions of X: we define X_- and X_+ as the NSZ and RSZ of X, respectively. The surface T delineates the topological sub-surfaces X_- and X_+ on X; T is a Mott insulator [30] and Fermi surface [41] which delineates two dual superconductors [30, 53, 59, 60, 67, 68]. Thus, $\forall x \in X$ we know that precisely one of the following conditions must be satisfied:

$$|x| < \epsilon_{2M} \Leftrightarrow x \in X_-, \tag{12}$$
$$|x| = \epsilon_{2M} \Leftrightarrow x \in T, \tag{13}$$
$$|x| > \epsilon_{2M} \Leftrightarrow x \in X_+, \tag{14}$$

where clearly $X_- \cap T = T \cap X_+ = X_- \cap X_+ = \emptyset$ and $X_- \cup T \cup X_+ = X$. Hence, T is the multiplicative group of all non-zero complex 1-vectors, such that

$$T = \{t \in X : |t| = \epsilon_{2M}\}, \tag{15}$$

where we define all T position-points as *time-points* and

$$X_- = \{s \in X : |s| < \epsilon_{2M}\}, \tag{16}$$
$$X_+ = \{s \in X : |s| > \epsilon_{2M}\}, \tag{17}$$

where we define all $S = X_- \cup X_+$ position-points as *space-points*. So clearly,

$$\epsilon_{2M}^2 = |t|^2 = |t_{\mathbb{R}}|^2 + |t_{\mathbb{I}}|^2, \quad \forall t \in T, \tag{18}$$
$$|x|^2 = |x_{\mathbb{R}}|^2 + |x_{\mathbb{I}}|^2, \quad \forall x \in X. \tag{19}$$

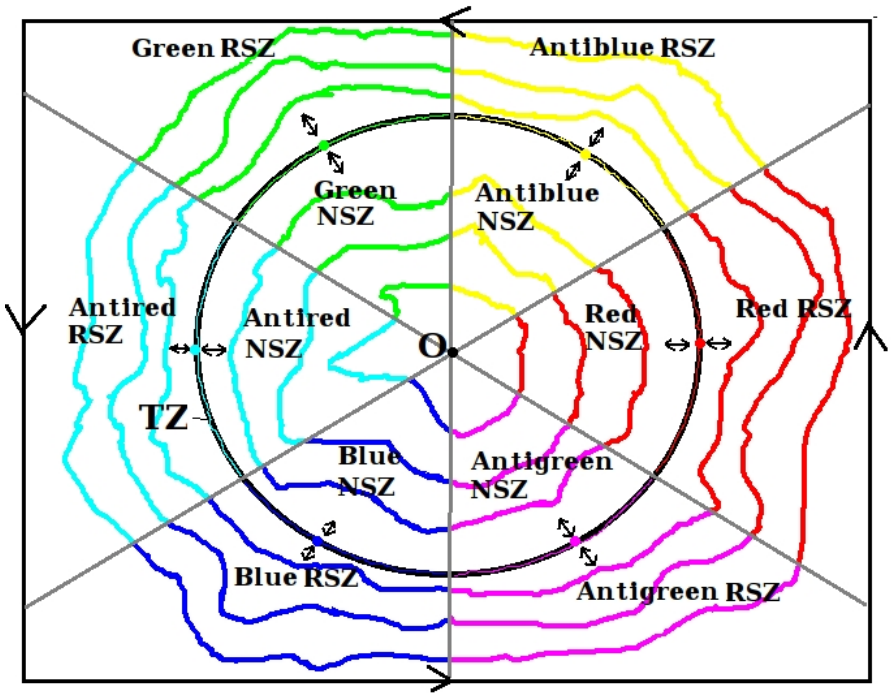

FIG. 5. The upgraded Gribov QCD/QED vacuum with 18 zones for quasiparticle signals pertaining to a BAB on the 1D Riemann surface. The $q\bar{q}$ pairs are confined to the TZ, which is dual to the NSZ and the RSZ. The six-coloring spinon, holon, and orbiton excitations are spontaneously generated and confined to the TZ, which acquires a geometric phase; the TZ excitations are dual to those of the NSZ and RSZ 3-branes.

So T is isometrically embedded in X with the one-to-one holographic mappings $f : T \hookrightarrow X$ and $f : T \to X_- \cup X_+$ with dual simultaneous bijections

$$f_{Time} : X_- \hookleftarrow T \hookrightarrow X_+, \tag{20}$$
$$f_{Space} : X_- \hookrightarrow T \hookleftarrow X_+, \tag{21}$$

for our dual space-time; we've proven that T is dual to X_- and T is also dual to X_+. Interestingly, this formulation may provide a simplification to the Riemann-Hilbert problem as expressed in, for example, [71]. Now because T is a type of Riemannian circle and holographic ring, we know it is a 2-sphere for the $SU(2)$ gauged Bose-Einstein condensate [29]. Thus, for the position-point and position-vector $t \in T$ we apply Definition (10) to express the 2-sphere generalized and synchronized 2D Riemann coordinates

$$^{2D}T : \ (t) = (t_{\mathbb{R}}+t_{\mathbb{I}}) = (t_{\mathbb{R}}, t_{\mathbb{I}}) = (|t|, \langle t \rangle) = (\epsilon, \langle t \rangle), \ \forall t \in T, \tag{22}$$

and in 3D Schwarzschild coordinates

$$^{3D}T : (u_t, |t|, \langle t \rangle) = (\frac{M}{|t|}, |t|, \langle t \rangle), \quad \forall t \in T. \tag{23}$$

Now because $\forall t \in T$ we have the uniform radius $|t| = \epsilon_{2M}$, we can alternatively drop the $|t|$ amplitude coordinate and just use the $\langle t \rangle$ phase coordinate to *directly* specify position-points on the 1D non-linear surface. Therefore, T is

- the *1D circular Abelian group* $U(1)$;
- the *2D spherical non-Abelian group* $SU(2)$; and
- isomorphic to the *3D orthogonal non-Abelian group* $SO(3)$,

which directly supports 1D, 2D, and 3D skyrmions [29]. So parity doubling [27] is synonymous of the term degeneracy, and Escher gave an example of how one can establish 2D - 3D correspondence [8]. We see here again the road to the t'Hooft and Maldacena holographic model for high-energy physics—all the 3D properties are inferred directly from the 2D (Riemannian holographic ring) domain [72].

We define T as a "fermiwire," which is nothing more than a "nanowire" [55, 73] with Rashba spin-orbit coupling [30, 32, 44] on the Fermi scale. The spin geometric phase for electrons in [32] is applied directly to the spin Hall effect [44], effective spin-dependent flux, and Andreev reflections [67, 68] of the quarks and antiquarks confined to the universal curve T (the holographic ring with uniform radius $|t| = \epsilon_{2M}$) embedded in X; the duality derivation between the AAS effect and the AC effect of [32] is written for T as $\frac{\Phi_{mag}}{\Phi_0/2} \iff \sqrt{1+\left(\frac{2m_t\langle t\rangle|t|}{\hbar^2}\right)^2}, \ \forall t \in T$, where Φ_{mag} is the magnetic flux, $\Phi_0 = h/e$ is the one flux quantum period, $\langle t \rangle = \alpha$ is the amplitude and strength of the Rashba spin-orbit interaction, and m_t is the effective mass; the left term is the

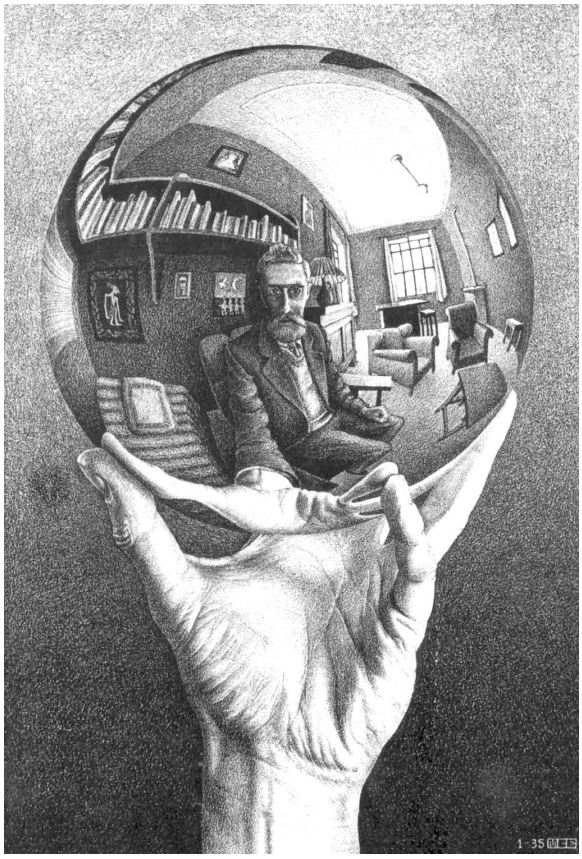

FIG. 6. The TZ is dual to *both* distance scales and imposes the double-confinement and double-lensing of M.C. Escher's duality [8]; it is a stereographic superlense [23] between the two 3-brane distance scales.

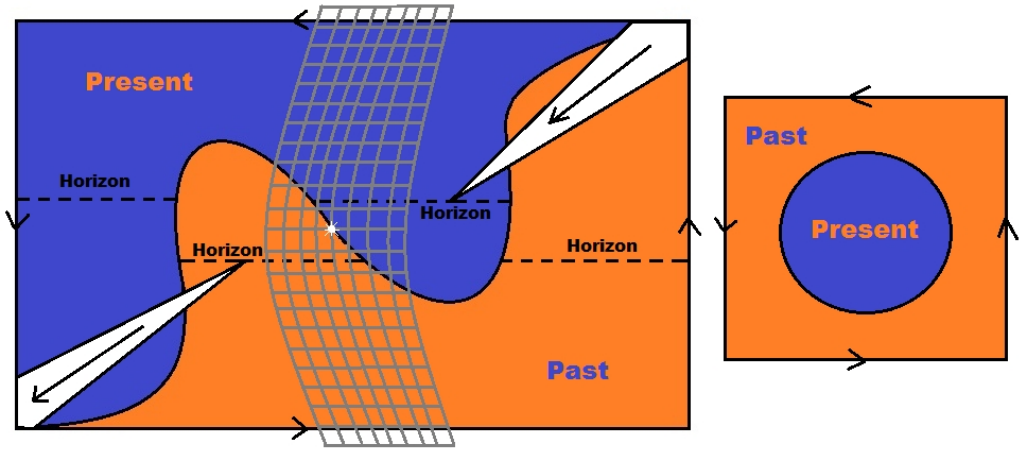

FIG. 7. Inopin's interpretation of M.C. Escher's double-horizons of [8] is directly connected to the $q \rightarrow \bar{q}$ transitions, past-present switching, time-reversal operation, and CPT-Theorem on the Riemann surface: time is circular and non-linear, so *the past is the future*. The quarks switch back and forth between the conjugate space-time regions with the appearance and disappearance of 3 quantum critical points in the QCD phase diagram.

AAS effect flux and the right term is the time-reversal AC effect oscillation unit with effective spin-dependent flux for the conductance modulation and voltage dependence observations of the AAS amplitude at zero magnetic field [32]. This formulation is crucial to our six-coloring quark-antiquark configuration for the BAC scenario because the magneto-resistance oscillations of [32, 74] along T are attributed to the AAS effect.

V. THE WAVEFUNCTION DEFINITION OF FRACTIONAL QUANTUM NUMBER ORDER PARAMETERS

Landau introduced the concept of OPs [2], which we define as complex scalar fields [10] on X. Here, we construct the BWF using OPs and Laughlin statistics [3] in our non-Abelian $SU(2)$ gauge theory. In the theory of superfluidity the OP measures the existence of Bose condensed particles (Cooper pairs) and is given by the probability amplitude of such particles. The inter-particle forces between quarks and antiquarks, and between ^{4}He and between ^{3}He atoms, are *rotationally invariant in spin and orbital space* and, of course, conserve quantum number [27]. The latter symmetry gives rise to gauge symmetry, which is *broken* in any superfluid. First, for the theory of *isotropic* superfluids like a BCS superconductor or superfluid ^{4}He, we define the *global* OP $\psi = \psi_{\mathbb{R}} + \psi_{\mathbb{I}}$ as a complex number (which inherits the notation similar to x as defined in Section III without loss of generality); ψ is both a complex scalar *and* Euclidean vector with the *amplitude* $|\psi|$ [14] and *phase* $\langle\psi\rangle$ components [10]. Then for *local* gauge SSB, we define the OP $\psi[x]$ as the complex scalar field

$$\psi[x] = \psi[x]_{\mathbb{R}} + \psi[x]_{\mathbb{I}}, \quad \forall x \in X, \tag{24}$$

where $|\psi[x]|$ and $\langle\psi[x]\rangle$ are the "gauge" amplitude and phase components local to $x \in X$, respectively, in accordance to Englert [10]. Furthermore, we define $\Delta|\psi[x]|$ and $\Delta\langle\psi[x]\rangle$ as the *change of* the OP's amplitude and phase due to a "massive Higgs-like *amplitude-excitation*" and "massless Nambu-Goldstone *phase-excitation*" components, respectively—see Figures 8 and 9. Since the Mott insulator and stereographic superlense T is dual to both $X-$ and X_+, we express Equation (24) specifically for time-points as the *parametric* function

$$\psi(t) = \psi(t)_{\mathbb{R}} + \psi(t)_{\mathbb{I}}, \quad \forall t \in T, \tag{25}$$

where the $SU(2)$ gauge-invariant T acquires a Berry–Aharonov–Anandan geometric phase as in [56]; T is an *ordered medium* equipped with an OP space for topological defects. The classical energy density distribution along T is a function of the OP $\psi(t)$; within the ordered (superfluid) phase, Nambu-Goldstone and Higgs modes arise from the $\langle\psi(t)\rangle$ and $|\psi(t)|$, respectively, where the energy density transforms into a function for T with a minimum at $|\psi(t)| = 0$ [14]. So $|\psi(t)|$ is excited with a periodic modulation of the spin-orbit coupling, which amounts to a "shaking" of the energy density (effective) potential for topological deformations along T in accordance with [14]. Furthermore, because the baryon-antibaryon pair is confined to T on the kagome lattice of antiferromagnetic ordering [43], we define the BWF for the six-coloring position-points $\{r, g, b\}$ *subset*T and $\{\bar{r}, \bar{g}, \bar{b}\} \subset T$ of three colored quarks and three anticolored antiquarks in the vacuum, respectively (recall Figures 3 and 4).

Above the critical temperature the system is invariant under an arbitrary change of the phase $\langle\psi[x]\rangle \to \langle\psi[x]\rangle'$, i.e. under a gauge transformation. Below the critical temperature a particular value of $\langle\psi\rangle$ is *spontaneously* preferred. In anisotropic superfluids, additional symmetries can be spontaneously broken, corresponding to *multiple* OP components of the BWF. In ^{3}He—the best studied example with multiple OP components—the pairs are in a spin-triplet state, meaning that rotational symmetry in spin space is broken, just as in a magnet. At the same time, the anisotropy of the Cooper-pair wavefunction in orbital space calls for a spontaneous breakdown of orbital rotation symmetry, as in *liquid crystals* [27]. Including the gauge symmetry, three symmetries are therefore broken in superfluid ^{3}He. The theoretical discovery that *several simultaneously broken symmetries* can appear in condensed matter was made by Antony Leggett, and represented a breakthrough in the theory of anisotropic superfluids, ^{3}He [2]. This leads to *superfluid phases* whose properties cannot be understood by simply adding the properties of systems in which each symmetry is *broken individually*. Such phases may have *long range* order in *combined*, rather than individual degrees of freedom. So to construct a strong BWF constraint for BAC to T, we "Cooper pair" the OP set of strongly conserved quantum numbers

$$\Phi_{OP} = \{\psi_C, \psi_I, \psi_J\}, \tag{26}$$

which is listed in Table I; the spin-orbit coupling of [44, 45, 65] applies directly to T, where $\psi_J(t)$ is identical to the "B_{SO}-vector" of [73], such that

$$\psi_J(t) = \psi_S(t) + \psi_L(t), \quad \forall t \in T. \tag{27}$$

The $q\bar{q}$ pairs confined to T on the six-coloring kagome lattice manifold are located at position-points $r, g, b, \bar{r}, \bar{g}, \bar{c} \in T$; they adhere to the uniformly-arranged position-point constraints

$$\langle r\rangle = \langle\bar{r}\rangle \pm \pi, \quad \langle g\rangle = \langle\bar{g}\rangle \pm \pi, \quad \text{and} \quad \langle b\rangle = \langle\bar{b}\rangle \pm \pi, \tag{28}$$

with uniform amplitudes $|r| = |g| = |b| = |\bar{r}| = |\bar{g}| = |\bar{b}| = \epsilon_{2M}$, and antiferromagnetic ordering

$$\langle\psi_J(r)\rangle = \langle\psi_J(\bar{r})\rangle \pm \pi, \tag{29}$$

$$\langle\psi_J(g)\rangle = \langle\psi_J(\bar{g})\rangle \pm \pi, \quad \text{and} \tag{30}$$

$$\langle\psi_J(b)\rangle = \langle\psi_J(\bar{b})\rangle \pm \pi, \tag{31}$$

(recall Figure 3). A little flight of imagination lead us to this new approach, where the OPs $\forall t \in T$ are "Cooper paired" to form a Leggett *superfluid B phase* of [2] with azimuthal "alpha" phase angle $\langle t\rangle$; the OPs $\forall\psi \in \Phi_{OP}$ rotate freely in 2D and 3D space, while the superfluid B phase angle $\langle t\rangle \in \{\langle r\rangle, \langle g\rangle, \langle b\rangle, \langle\bar{r}\rangle, \langle\bar{g}\rangle, \langle\bar{b}\rangle\}$ between them remains *constant*. Such phases form correlated helices along T, serving as constraints for the BWF—see Figure 10.

Next, we construct our BWF for the BAB states. For a baryon and antibaryon centered on the origin-point

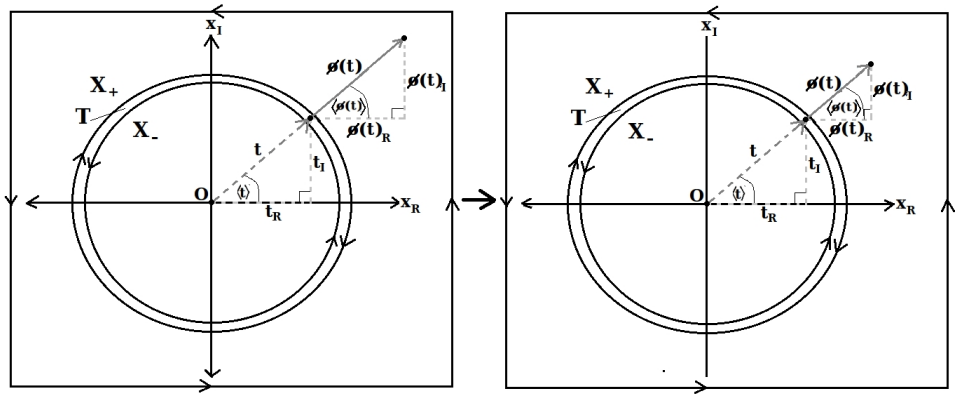

FIG. 8. A complex scalar field $\psi(t)$ experiences a massive "Higgs-like" *amplitude-excitation* [14] (right), which is characteristic of the Nambu-Goldstone *scalar* boson SSB order parameter fluctuations discussed by [10]; a classical wave imposes volume effects and stretches the vacuum field.

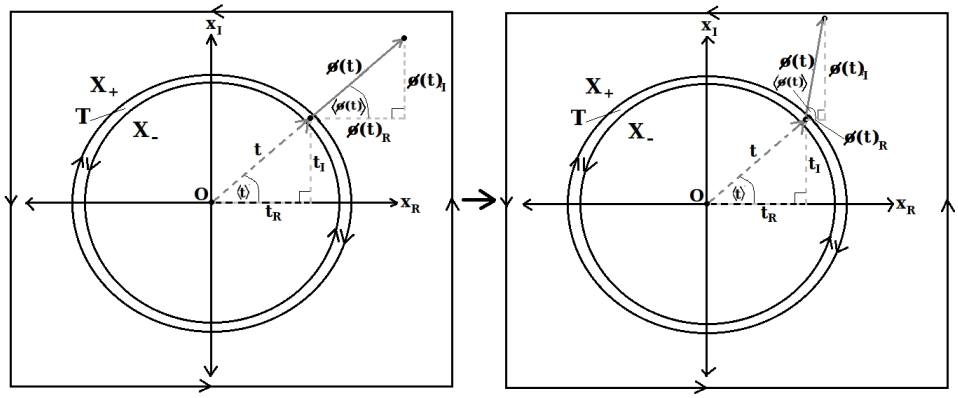

FIG. 9. A complex scalar field $\psi(t)$ experiences a *phase-excitation* (right), which is characteristic of the Nambu-Goldstone *pseudo-scalar* SSB order parameter fluctuations discussed by [10]; a classical wave imposes rotational effects on the vacuum field in accordance with vacuum degeneracy.

$O \in X$ and confined to T we define the *full* baryon and antibaryon states as

$$\Psi_{total}(r,g,b) = \Psi(r) \times \Psi(g) \times \Psi(b) \quad \text{and} \tag{32}$$

$$\Psi_{total}(\bar{r},\bar{g},\bar{b}) = \Psi(\bar{r}) \times \Psi(\bar{g}) \times \Psi(\bar{b}), \tag{33}$$

respectively, for the BAC and BAD; the *red*, *green*, and *blue* quark wavefunctions respectively located at time-points $r, g, b \in T$ on the three-coloring triangular sub-lattice are

$$\Psi(r) = \psi_C(r) \times \psi_J(r) \times \psi_I(r) \times r, \quad \Psi(r) \stackrel{def}{=} \langle r|\Psi\rangle, \tag{34}$$

$$\Psi(g) = \psi_C(g) \times \psi_J(g) \times \psi_I(g) \times g, \quad \Psi(g) \stackrel{def}{=} \langle g|\Psi\rangle, \tag{35}$$

$$\Psi(b) = \psi_C(b) \times \psi_J(b) \times \psi_I(b) \times b, \quad \Psi(b) \stackrel{def}{=} \langle b|\Psi\rangle, \tag{36}$$

and the *antired*, *antigreen*, and *antiblue* antiquark wavefunctions respectively located at time-points $\bar{r}, \bar{g}, \bar{b} \in T$ on the three-anticoloring triangular sub-lattice are

$$\Psi(\bar{r}) = \psi_C(\bar{r}) \times \psi_J(\bar{r}) \times \psi_I(\bar{r}) \times \bar{r}, \quad \Psi(\bar{r}) \stackrel{def}{=} \langle \bar{r}|\Psi\rangle, \tag{37}$$

$$\Psi(\bar{g}) = \psi_C(\bar{g}) \times \psi_J(\bar{g}) \times \psi_I(\bar{g}) \times \bar{g}, \quad \Psi(\bar{g}) \stackrel{def}{=} \langle \bar{g}|\Psi\rangle, \tag{38}$$

$$\Psi(\bar{b}) = \psi_C(\bar{b}) \times \psi_J(\bar{b}) \times \psi_I(\bar{b}) \times \bar{b}, \quad \Psi(\bar{b}) \stackrel{def}{=} \langle \bar{b}|\Psi\rangle; \tag{39}$$

the BWF for the three distinct $q\bar{q}$ pairs that are confined to T along the six-coloring kagome lattice manifold (recall Figure 3). So the antisymmetric BWF is described with the six-coloring components

$$\Psi(r,\bar{r}) = -\Psi(\bar{r},r), \tag{40}$$

$$\Psi(g,\bar{g}) = -\Psi(\bar{g},g), \quad \text{and} \tag{41}$$

$$\Psi(b,\bar{b}) = -\Psi(\bar{b},b), \tag{42}$$

for the confined quark and antiquark (two-particle) cases.

So for Definition (32) and the related six-coloring Definitions (31–37), we define the full BWF antisymmetriza-

TABLE I. The quantum number order parameters for the BWF states on the 1D Riemann surface X. Here, $\psi_J = \psi_S + \psi_L$ and $\psi_J(t) = \psi_S(t) + \psi_L(t)$ for the spin-orbit coupling of the holographic confinement ring $T \subset X$.

Order Parameter	Symbol	Global	Local
Color Charge	C	$\psi_C = \psi_{C_{\mathbb{R}}} + \psi_{C_{\mathbb{I}}}$	$\psi_C[x] = \psi_C[x]_{\mathbb{R}} + \psi_C[x]_{\mathbb{I}}$
Isospin	I	$\psi_I = \psi_{I_{\mathbb{R}}} + \psi_{I_{\mathbb{I}}}$	$\psi_I[x] = \psi_I[x]_{\mathbb{R}} + \psi_I[x]_{\mathbb{I}}$
Orbital Angular Momentum	L	$\psi_L = \psi_{L_{\mathbb{R}}} + \psi_{L_{\mathbb{I}}}$	$\psi_L[x] = \psi_L[x]_{\mathbb{R}} + \psi_L[x]_{\mathbb{I}}$
Spin Angular Momentum	S	$\psi_S = \psi_{S_{\mathbb{R}}} + \psi_{S_{\mathbb{I}}}$	$\psi_S[x] = \psi_S[x]_{\mathbb{R}} + \psi_S[x]_{\mathbb{I}}$
Total Angular Momentum	J	$\psi_J = \psi_{J_{\mathbb{R}}} + \psi_{J_{\mathbb{I}}}$	$\psi_J[x] = \psi_J[x]_{\mathbb{R}} + \psi_J[x]_{\mathbb{I}}$

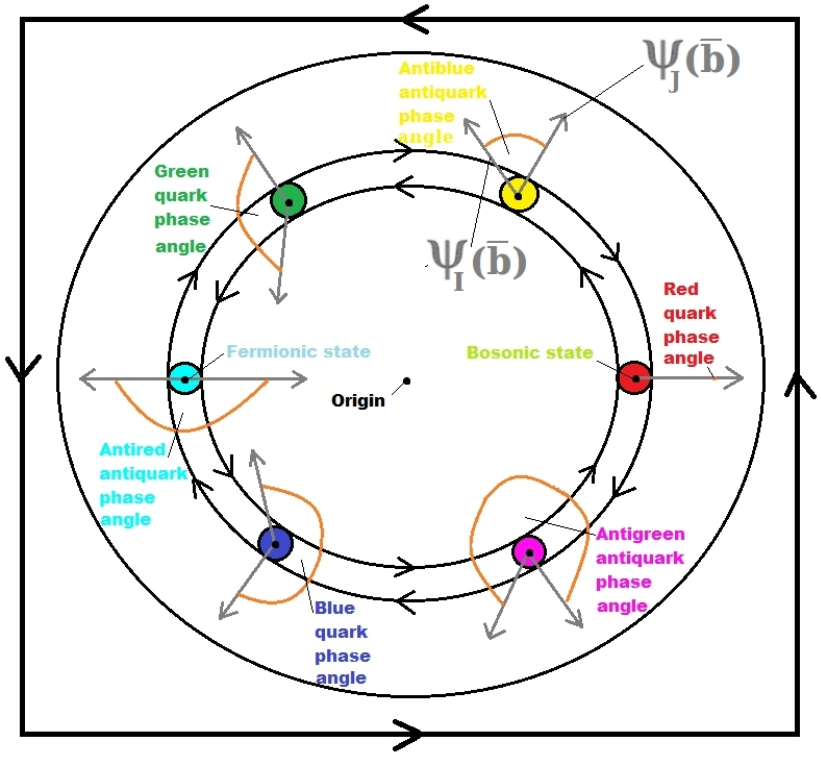

FIG. 10. Leggett's [2] six distinct superfluid B phase angles for the three $q\bar{q}$ pairs confined to T along the six-coloring kagome lattice of antiferromagnetic ordering [3, 43]. The superfluid B phase angles $\langle r\rangle, \langle g\rangle, \langle b\rangle, \langle \bar{r}\rangle, \langle \bar{g}\rangle, \langle \bar{b}\rangle$ remain *constant* and correlate the OPs as they rotate freely in 2D and 3D space; this *long range order* applies $\forall t \in T$, $\forall \psi \in \Phi_{OP}$, to form correlated helices along T; this concept serves as a strong BWF constraint and applies to all OPs for a given time-point. In this diagram, only $\psi_J(t)$ and $\psi_I(t)$ are shown, but $\psi_C(t)$ is also correlated with $\langle t\rangle$.

tion via the covariant antisymmetric metric tensor: the 2D antisymmetric BWF matrix

$$\begin{pmatrix} 0 & \Psi_{total}(r,g,b) \\ \Psi_{total}(\bar{r},\bar{g},\bar{b}) & 0 \end{pmatrix} \tag{43}$$

and the expanded 3D antisymmetric BWF matrix

$$\begin{pmatrix} 0 & \Psi(r) & \Psi(g) \\ \Psi(\bar{r}) & 0 & \Psi(b) \\ \Psi(\bar{g}) & \Psi(\bar{b}) & 0 \end{pmatrix} \tag{44}$$

for T. So given complex tangent vectors μ and ν we define

$$g_x(\mu,\nu) = -g_x(\nu,\mu) \in \mathbb{C}, \quad \forall x \in X; \tag{45}$$

the tensor describes the X curvature ("vector phase") $\langle g_x(\mu,\nu)\rangle$ and the field strength ("vector amplitude") $|g_x(\mu,\nu)|$ at a position-point $x \in X$. The Levi-Civita symbol for the color singlet function is

$$\zeta_{rgb} = \zeta^{rgb} = \begin{cases} +1 \text{ if } (r,g,b) \text{ is } (1,2,3),\ (2,3,1),\ \text{or } (3,1,2) \\ 0 \text{ if } r=g \text{ or } g=b \text{ or } b=r \\ -1 \text{ if } (r,g,b) \text{ is } (3,2,1),\ (2,1,3),\ \text{or } (1,3,2) \end{cases} \tag{46}$$

The CPT-Theorem is a fundamental property of T. Hence, for a baryon or antibaryon of scale M we have

the OP *charge transformation(s)*, $\forall \psi \in \Phi_{OP}$,

$$C : \begin{cases} \psi(t) & \mapsto -\psi(t), \\ \begin{pmatrix} \psi(t)_{\mathbb{R}} \\ \psi(t)_{\mathbb{I}} \end{pmatrix} & \mapsto \begin{pmatrix} -\psi(t)_{\mathbb{R}} \\ -\psi(t)_{\mathbb{I}} \end{pmatrix}, \\ \begin{pmatrix} |\psi(t)| \\ \langle \psi(t) \rangle \end{pmatrix} & \mapsto \begin{pmatrix} |\psi(t)| \\ \langle \psi(t) \rangle \pm \pi \end{pmatrix}, \end{cases} \tag{47}$$

the *parity transformation(s)* (in generalized 2D Riemann coordinates for 3D Schwarzschild space) is the flip in the sign of the one coordinate

$$P : \begin{cases} \begin{pmatrix} t_{\mathbb{R}} \\ t_{\mathbb{I}} \\ \frac{M}{|t|} \end{pmatrix} & \mapsto \begin{pmatrix} -t_{\mathbb{R}} \\ -t_{\mathbb{I}} \\ -\frac{M}{|t|} \end{pmatrix}, \\ \begin{pmatrix} |t| \\ \langle t \rangle \\ \frac{M}{|t|} \end{pmatrix} & \mapsto \begin{pmatrix} |t| \\ \langle t \rangle \pm \pi \\ -\frac{M}{|t|} \end{pmatrix}, \end{cases} \tag{48}$$

and *time reversal transformation(s)*

$$T : \begin{cases} t & \mapsto -t, \\ \begin{pmatrix} t_{\mathbb{R}} \\ t_{\mathbb{I}} \end{pmatrix} & \mapsto \begin{pmatrix} -t_{\mathbb{R}} \\ -t_{\mathbb{I}} \end{pmatrix}, \\ \begin{pmatrix} |t| \\ \langle t \rangle \end{pmatrix} & \mapsto \begin{pmatrix} |t| \\ \langle t \rangle \pm \pi \end{pmatrix}, \end{cases} \tag{49}$$

which comprise a CPT-transformation, $\forall t \in T$. We see that for Definitions (47), (48), and (49) there are multiple equivalent transformations for each case because the generalized Riemann coordinates of Definition (10) and the OP Definition (24) use synchronized Complex-Cartesian-Polar values (where the magnitude and direction of the Polar components are replaced with amplitude and phase, respectively).

VI. THE LAGRANGIAN: EFFECTIVE POTENTIAL AND EFFECTIVE KINETIC

Here, we express the gauged SSB in our FQHS space-time scenario on X, which is applicable to both 2D and 3D space; the Lagrangian is defined as

$$\mathcal{L}[x] = E_K[x] - E_P[x], \quad \forall x \in X, \tag{50}$$

using our generalized coordinates, where $E_K[x]$ and $E_P[x]$ are the *effective kinetic* and *effective potential*, respectively, for a position-point x. From [75] the gauge boson's E_P is defined as

$$E_P[x] = \frac{\sqrt{1-2u_x}}{|x|}, \quad \forall x \in X. \tag{51}$$

The E_P depends on the Schwarzschild geometry but not on the choice of orbit. Only one E_P is required to analyze the motion of all radiation (including radio waves, radar pulses, gamma rays, etc.). It is important to stress E_P differences and similarities between a massive particle and its massless limit: radiation-rays. Next, the E_K is defined as

$$E_K[x] = \frac{1}{2} m_x v_x^2 = \frac{1}{2} \frac{F_x}{a_x} v_x^2, \quad \forall x \in X, \tag{52}$$

where F_x is the *effective force*, where m_x is the *effective mass*, a_x is the *effective acceleration*, and v_x is the *effective velocity* of the particle at x in the FQHS space-time. Einstein's F_x, the E_P *per unit of particle effective mass* m_x, is defined as

$$F_x = m_x a_x = \frac{E_P[x]}{m_x} = \sqrt{(1-2u_x)\left[1 + \frac{(\frac{J}{m_x})^2}{|x|^2}\right]}, \quad \forall x \in X, \tag{53}$$

where the a_x along coordinate phase $\langle x \rangle$ is

$$a_x = \frac{1}{\hbar^2} \sum_{m_x} \frac{\partial^2 \varepsilon(k_x)}{\partial k_{\langle x \rangle} \partial k_{m_x}} e_x E_{m_x}, \quad \forall x \in X, \tag{54}$$

where k_x is the wave vector, $\varepsilon(k_x)$ is the dispersion relation, and e_x is the point charge in an external electric field E.

VII. A BRIEF CORRESPONDENCE TO YUAN, MO, AND WANG

So now that we've presented our model, we realize that it inherits exceptional components from the YMW baryon-antibaryon $SU(3)$ model [17]; in particular, it is evident that their ideas and applied methodology strongly support our BAC proof. Here, we compare and contrast our model with the YMW model and provide a brief correspondence aimed at unifying the conceptual and mathematical components of both schemes. We've identified the YMW model as a well-defined framework that provides crucial insight into the nature of (theoretical and experimental) particle physics. Moreover, we've found that the construction of our BAC proof has inevitably led us to assemble a theory and framework that effectively replicates core expressions of the YMW paradigm, bringing us along similar paths of exploration.

To summarize, the YMW model is a nonet scheme which predicts many new baryon-antibaryon bound states and their possible productions in quarkonium decays and B decays [17]. It is designed to classify the increased number of experimentally observed enhancements near the baryon-antibaryon threshold. It is largely based on the Fermi-Yang-Sakata (FYS) model [76, 77], in which mesons were interpreted as baryon-antibaryon bound states [17]. The discovery of the increased number of baryon-antibaryon enhancements near thresholds reminds the YMW authors of the era prior to the development of the $SU(3)$ quark model over half a century ago,

when the so-called elementary particles emerged one-by-one [17]. So YMW return to the FYS model and extend various aspects of it.

First, we identify a few key *similarities* between our model and the YMW model [17]. In short, both schemes:

- Share the core hexagon structure equipped with a baryon-antibaryon pair.
- Intertwine a hexagon and circle(s) to encode certain fundamental aspects of the baryon-antibaryon state space.
- Predict many new baryon-antibaryon bound states.
- Accommodate the enhancements near the baryon-antibaryon mass thresholds.
- Predict the increase and decrease of masses for the dual three-quark system (the baryon and the antibaryon) with respect the baryon-antibaryon mass threshold.
- Organize quark-antiquark pairs into flavorless mesons.
- Account for pseudo-scalar meson states.
- Support the possible charmonium and B decay modes as listed by YMW.

Second, we identify a few key *dissimilarities* between our model and the YMW model [17]. In doing so, we clarify that our model is not only consistent with the YMW model, but upgrades many of its components by simplifying the nonet representation from $SU(3)$ to $SU(2)$ and extending its state space, accuracy, and predictive capability. In short, the schemes differ in that:

- The hexagon structure of the YMW model does not incorporate the six-coloring kagome lattice antiferromagnet, whereas our model does; but the YMW model can be equipped with this powerful lattice structure to fundamentally enhance its representational capability.
- The YMW model does not model the quarks as coupled oscillators which generate effective mass, whereas our model does; but the YMW model can be equipped with quark coupled oscillators to attribute its mass increases and decreases to the effective mass generated by the interconnected oscillators.
- The YMW model employs classic *quantum numbers* (for total angular momentum, isospin, strangeness, and charge) to encode the system state, whereas our model employs *quantum number OPs* (for total angular momentum, isospin, and color charge) to encode the system state with additional precision; but the YMW model can be equipped with quantum number OPs of fractional statistics to construct a well-defined (baryon and antibaryon) wavefunction in state space, where the OPs are correlated with superfluid B phases [2].
- The YMW model only accounts for pseudo-scalar mesons, whereas our model accounts for pseudo-scalar *and* scalar mesons, while directly associating these components to massless Nambu-Goldstone phase-excitations [11–13] and massive Higgs-like amplitude-excitations [14], respectively; but the YMW model can be equipped with scalar mesons, phase-excitations, and amplitude-excitations that correspond to a "Goldstone Family" of gauge bosons for SSB.
- The YMW model does not define a Lagrangian that is consistent with Newtonian *and* Einsteinian paradigms in 4D space-time, whereas ours does; but the YMW model can be simplified and formulated as such to highlight these additional space-time and dynamical system relationships.
- The circular structures of the YMW model do not consider a well-defined circular dimension of time that is modeled as a Riemannian holographic ring unit circle, stereographic gravitational superlense [23], Gedanken interferometer [62], and Mott insulator [30] that is dual to both superconducting 3-branes which simultaneously triggers CPT-violations on the dual distance scales, whereas ours model does employ these notions; but the YMW model can be equipped with this paradigm so it is consistent with, for example, M.C. Escher's duality [8].
- The YMW model is not based upon a dual space-time topology equipped with topological deformations of intertwined superluminal (non-relativistic) signals and luminal (relativistic) signals, whereas our model does incorporate this arrangement; but the YMW model can be equipped with such energy deformations, signal classifications, and topological structure.

At this point we've provided a brief report that compares and contrasts some high-level aspects between the two models. For the future, this suggests that we may clarify a plethora of new ideas and fundamental relationships through an objective consolidation of both frameworks.

VIII. CONCLUSION AND OUTLOOK

In this first paper of the series, we introduced the topologies, vacuum, generalized coordinates, fractional statistics, BWF quantum number OPs, gauge symmetry breaking, and Lagrangian for our BAC proof and BAD in 4D FQHS space-time that complies with Newtonian and Einsteinian mechanics, and low-dimensional

implementations of string theory and M-theory. In the next paper(s) of this series, we will extend our quark-antiquark confinement scenario by discussing the anyons, phase locking, HH, attractive and repulsive gravitational effects of quasiparticle signals on the Lagrangian, modified Gullstrand–Painlevé reference frames, and Magnification Effect.

In our opinion, this proof of quark-antiquark confinement with the amplitude–excitations and phase–excitations begins to reveal additional fundamental mechanisms and relationships inherent to our universe. In doing so, we've been able to shed more light on a number of mysterious concepts in nature, including antibaryons, baryons, baryon asymmetry, creation, annihilation, double horizons, and FQHS space-time. We suspect that these formulations, which are inspired by a plethora of experimental data, can be used to construct a unified field theory in the near future, thereby advancing physics to the "next level." Through global cooperation, competition, hard work, and creativity, these powerful concepts can be further scrutinized, extended, and applied to virtually all areas of mathematics, science, medicine, and engineering.

[1] V. Barger and R. Phillips. *Collider physics*. Addison-Wesley publishing company, 1997.

[2] A. Reading. Leggett, aj: A theoretical description of the new phases of liquid he. *Rev. Mod. Phys*, 47:331, 1975.

[3] R.B. Laughlin. Parallels between quantum antiferromagnetism and the strong interactions. *Arxiv preprint cond-mat/9802180*, 1998.

[4] I. Newton, D. Bernoulli, C. MacLaurin, and L. Euler. *Philosophiæ naturalis principia mathematica*, volume 1. excudit G. Brookman; impensis TT et J. Tegg, Londini, 1833.

[5] K.S. Thome. *Black Holes and Time Warps: Einstein's outrageous legacy*. New York: WW Norton&Company, 1994.

[6] T.P. Cheng, L.F. Li, and T.P. Cheng. *Gauge theory of elementary particle physics*. Clarendon Press Oxford, 1984.

[7] K. Becker, M. Becker, and J.H. Schwarz. *String theory and M-theory: A modern introduction*. Cambridge University Press, 2006.

[8] M.C. Escher, B. Ernst, and J.E. Brigham. *The magic mirror of MC Escher*. Random House, 2007.

[9] F.E. Camino, W. Zhou, and V.J. Goldman. Realization of a Laughlin quasiparticle interferometer: observation of fractional statistics. *Physical Review B*, 72(7):075342, 2005.

[10] F. Englert. Symmetry breaking and the scalar boson - evolving perspectives. *Arxiv preprint hep-th/1204.5382v1*, 2012.

[11] J. Goldstone. Broken symmetries. *Selected papers of Abdus Salam:(with commentary)*, 5:204, 1994.

[12] Y. Nambu. Axial vector current conservation in weak interactions. *Physical Review Letters*, 4(7):380–382, 1960.

[13] Y. Nambu and G. Jona-Lasinio. Dynamical model of elementary particles based on an analogy with superconductivity. i. *Physical Review*, 122(1):345, 1961.

[14] M. Endres, T. Fukuhara, D. Pekker, M. Cheneau, P. Schauβ, C. Gross, E. Demler, S. Kuhr, and I. Bloch. The 'Higgs' amplitude mode at the two-dimensional superfluid/Mott insulator transition. *Nature*, 487(7408):454–458, 2012.

[15] E. Witten. Black holes and quark confinement. *Current Science-Bangalore-*, 81(12):1576–1581, 2001.

[16] R.B. Laughlin. Fractional quantization. *Nobel lectures, physics, 1996-2000*, page 264, 2002.

[17] C.Z. Yuan, XH Mo, and P. Wang. Baryon–antibaryon nonets. *Physics Letters B*, 626(1):95–100, 2005.

[18] D.O. Pushkin, D.E. Melnikov, and V.M. Shevtsova. Ordering of small particles in one-dimensional coherent structures by time-periodic flows. *Physical Review Letters*, 106(23):234501, 2011.

[19] Q.H. Hu. The nature of the electron. *Arxiv preprint physics/0512265*, 2005.

[20] M.J. Thoraval, K. Takehara, T.G. Etoh, and et al. Popinet, S. von Kármán vortex street within an impacting drop. *Phys. Rev. Lett.*, 108:264506, Jun 2012.

[21] R.A. Shelby, D.R. Smith, S.C. Nemat-Nasser, and S. Schultz. Microwave transmission through a two-dimensional, isotropic, left-handed metamaterial. *Applied Physics Letters*, 78:489, 2001.

[22] J. Li and C.T. Chan. Double-negative acoustic metamaterial. *Physical Review E*, 70(5):055602, 2004.

[23] U. Leonhardt. Perfect imaging without negative refraction. *New Journal of Physics*, 11:093040, 2009.

[24] V.G. Veselago and E.E. Narimanov. The left hand of brightness: past, present and future of negative index materials. *Nature materials*, 5(10):759–762, 2006.

[25] W. Melnitchouk, R. Ent, and C.E. Keppel. Quark–hadron duality in electron scattering. *Physics reports*, 406(3):127–301, 2005.

[26] B.Z. Kopeliovich, B. Povh, and I. Schmidt. Glue drops inside hadrons. *arXiv:hep-ph/0607337v1 [hep-ph]*, 2006.

[27] A.E. Inopin. Parity doublers and topology twists in hadrons. In *AIP Conference Proceedings*, volume 1030, page 298, 2008.

[28] P. Zhang, P. Horvathy, and J. Rawnsley. Topology, and (in)stability of non-Abelian monopoles. *Annals of Physics*, 327:118–165, 2012.

[29] T. Kawakami, T. Mizushima, M. Nitta, and K. Machida. Stable skyrmions in SU(2) gauged Bose-Einstein condensates. *Phys. Rev. Lett.*, 109:015301, Jul 2012.

[30] J. Schlappa, K. K. Wohlfeld, Zhou J., and et al. Mourigal, M. Spin-orbital separation in the quasi-one-dimensional mott insulator Sr2CuO3. *Nature*, 2012.

[31] Y. Aharonov and J. Anandan. Phase change during a cyclic quantum evolution. *Physical Review Letters*, 58(16):1593–1596, 1987.

[32] F. Nagasawa, J. Takagi, and et al. Kunihashi, Y. Experimental demonstration of spin geometric phase: Radius dependence of time-reversal Aharonov-Casher oscillations. *Physical Review Letters*, 108(12):086801, 2012.

[33] K. Richter. The ABC of Aharonov effects. *Physics*, 5:22, Feb 2012.

[34] M.G. Olsson. *arXiv:hep-ph/0001227*, 2000.
[35] S. Todorova. About the helix structure of the Lund string. *Arxiv preprint arXiv:1101.2407*, 2011.
[36] S. Todorova. Study of the helix structure of QCD string. *arXiv:1204.2655v1 [hep-ph]*, 2012.
[37] P.P. Cortet, A. Chiffaudel, F. Daviaud, and B. Dubrulle. Experimental evidence of a phase transition in a closed turbulent flow. *Physical review letters*, 105(21):214501, 2010.
[38] C.N. Varney, K. Sun, V. Galitski, and M. Rigol. Kaleidoscope of exotic quantum phases in a frustrated xy model. *Physical Review Letters*, 107(7):77201, 2011.
[39] D.A. Siegel, C.H. Park, C. Hwang, and et al. Deslippe, J. Many-body interactions in quasi-freestanding graphene. *Proceedings of the National Academy of Sciences*, 108(28):11365, 2011.
[40] A. Paramekanti, L. Balents, and M. Fisher. Ring exchange, the bose metal, and bosonization in two dimensions. *Arxiv preprint cond-mat/0203171*, 2002.
[41] F.E. Close, Y.L. Dokshitzer, V.N. Gribov, and et al. Khoze, V.A. Eye-witnesses of confinement. *Physics Letters B*, 319(1):291–299, 1993.
[42] Y.M. Tousi, V. Pourahmad, and E. Afshari. Delay coupled oscillators for frequency tuning of solid-state terahertz sources. *Physical Review Letters*, 108(23):234101, 2012.
[43] O. Cépas and A. Ralko. Resonating color state and emergent chromodynamics in the kagome antiferromagnet. *Physical Review B*, 84(2):020413, 2011.
[44] S. Souma and B.K. Nikolić. Spin hall current driven by quantum interferences in mesoscopic rashba rings. *Physical review letters*, 94(10):106602, 2005.
[45] T.W. Chen and G.Y. Guo. Torque and conventional spin Hall currents in two-dimensional spin-orbit coupled systems: Universal relation and hyperselection rule. *Physical Review B*, 79(12):125301, 2009.
[46] Catherine Pappas. New twist in chiral magnets. *Physics*, 5:28, Mar 2012.
[47] K. Marty, V. Simonet, E. Ressouche, and et al. Ballou, R. Single domain magnetic helicity and triangular chirality in structurally enantiopure Ba3NbFe3Si2o14. *Arxiv preprint arXiv:0809.3067*, 2008.
[48] E. Edlund, O. Lindgren, and M.N. Jacobi. Chiral surfaces self-assembling in one-component systems with isotropic interactions. *Phys. Rev. Lett.*, 108:165502, Apr 2012.
[49] A. Bostwick, F. Speck, T. Seyller, and et al. Horn, K. Observation of plasmarons in quasi-freestanding doped graphene. *Science*, 328(5981):999–1002, 2010.
[50] A. Principi, R. Asgari, and M. Polini. Acoustic plasmons and composite hole-acoustic plasmon satellite bands in graphene on a metal gate. *Solid State Communications*, 2011.
[51] A.E. Inopin. Comment to the review by L. Glozman, hep-ph/0701081. *arXiv:hep-ph/0702257v1 [hep-ph]*, 2007.
[52] P. Engels. Observing the dance of a vortex- antivortex pair, step by step. *Physics*, 3:33, 2010.
[53] D. Sticlet, C. Bena, and P. Simon. Spin and Majorana polarization in topological superconducting wires. *Physical Review Letters*, 108(9):096802, 2012.
[54] C.H.L. Quay, T.L. Hughes, J.A. Sulpizio, and L.N. et al. Pfeiffer. Observation of a one-dimensional spin–orbit gap in a quantum wire. *Nature Physics*, 6(5):336–339, 2010.
[55] S. Nadj-Perge, V.S. Pribiag, and et al. Berg, J.W.G. Spectroscopy of spin-orbit quantum bits in indium antimonide nanowires. *Physical Review Letters*, 2012.
[56] P. Bruno. Quantum geometric phase in Majorana's stellar representation: Mapping onto a many-body Aharonov-Bohm phase. *Phys. Rev. Lett*, 108:240402, 2012.
[57] M.N. Chernodub. Superconductivity of qcd vacuum in strong magnetic field. *Physical Review D*, 82(8):085011, 2010.
[58] E.B. Sonin. Magnus force in superfluids and superconductors. *Physical Review B*, 55(1):485, 1997.
[59] L. Fu and C.L. Kane. Superconducting proximity effect and Majorana fermions at the surface of a topological insulator. *Physical review letters*, 100(9):96407, 2008.
[60] J.D. Sau, R.M. Lutchyn, S. Tewari, and S. Das Sarma. Generic new platform for topological quantum computation using semiconductor heterostructures. *Physical review letters*, 104(4):40502, 2010.
[61] V.N. Gribov. *Eur. Phys. J. C 10*, pages 91–105, 1999.
[62] V. Jacques, F. Grosshans, F. Treussart, and P. Grangier. Experimental realization of Wheeler's delayed-choice gedanken experiment. *Science Magazine*, 315(5814):966–968, 2007.
[63] H. Pfau, S. Hartmann, U. Stockert, and et al. Sun, P. Thermal and electrical transport across a magnetic quantum critical point. *Nature*, 484(7395):493–497, 2012.
[64] J. Friedman, M.S. Morris, I.D. Novikov, and F. et al. Echeverria. Cauchy problem in spacetimes with closed timelike curves. *Physical Review D*, 42(6):1915, 1990.
[65] F. Wilczek. Magnetic flux, angular momentum, and statistics. *Physical Review Letters*, 48(17):1144–1146, 1982.
[66] D. Faccio. Laser pulse analogues for gravity and analogue Hawking radiation. 2011.
[67] X. Du, I. Skachko, and E.Y. Andrei. Josephson current and multiple Andreev reflections in graphene sns junctions. *Physical Review B*, 77(18):184507, 2008.
[68] H. Nilsson, P. Samuelsson, P. Caroff, and H. Xu. Supercurrent and multiple Andreev reflections in an insb nanowire Josephson junction. *Nano Letters*, 2012.
[69] V.V. Anisovich, D.V. Bugg, and A.V. Sarantsev. Exotic mesons, locking states, and their role in the formation of the confinement barrier. *Physical Review D*, 58(11):111503, 1998.
[70] V. Bangert, C. Croke, S. Ivanov, and M. Katz. Filling area conjecture and ovalless real hyperelliptic surfaces. *Geometric and Functional Analysis*, 15(3):577–597, 2005.
[71] A. Its. The Riemann-Hilbert problem and integrable systems. *Notices of the AMS*, 50(11):1389–1400, 2003.
[72] J. Maldacena. The illusion of gravity. *Scientific American*, 11:57–63, 2005.
[73] V. Mourik, K. Zuo, S.M. Frolov, and et al. Plissard, S.R. Signatures of Majorana fermions in hybrid superconductor-semiconductor nanowire devices. *Arxiv preprint arXiv:1204.2792*, 2012.
[74] B. Pannetier, J. Chaussy, R. Rammal, and P. Gandit. First observation of Altshuler-Aronov-Spivak effect in gold and copper. *Phys. Rev. B*, 31:3209–3211, Mar 1985.
[75] E.F. Taylor and J.A. Wheeler. Exploring black holes: introduction to general relativity. *Recherche*, 67:02, 2000.
[76] E. Fermi and C.N. Yang. Are mesons elementary particles? *Physical Review*, 76:1739–1743, 1949.
[77] S. Sakata. On a composite model for the new particles. *Progress of theoretical physics*, 16(6):686–688, 1956.